Q. J. R. Meteorol. Soc. (1999), **125**, pp. 2379–2400

Retrieval of surface and atmospheric parameters over land from SSM/I: Potential and limitations

By C. PRIGENT[1]* and W. R. ROSSOW[2]
[1]*Columbia University, USA*
[2]*NASA Goddard Institute for Space Studies, USA*

(Received 18 September 1998; revised 19 January 1999)

SUMMARY

The potential to retrieve surface temperature, water vapour content and cloud liquid water path from the Special Sensor Microwave/Imager (SSM/I) observations over land is examined, using a variational inversion scheme. The method relies upon prior estimates of the monthly mean land surface microwave emissivities and exploits a priori information on the atmospheric situation (International Satellite Cloud Climatology Project (ISCCP) data and National Center for Environmental Prediction analysis). The accuracy of the surface temperature retrieval is of the order of 1 K, does not strongly depend on surface type and is not very sensitive to the presence of thin clouds. The sensitivity to the water vapour is very low except in the most arid areas. With an accuracy of ~ 0.1 kg m^{-2}, the SSM/I retrieval does not properly characterize thin clouds, but the major cloud structures are well delineated and qualitative agreement is observed between the SSM/I and ISCCP estimations. This inversion process also has some ability to detect rain events.

KEYWORDS: Microwave Radiative transfer Variational inversion

1. INTRODUCTION

The use of satellite microwave observations to retrieve atmospheric parameters has generally been limited to ocean areas because the ocean surface has a low microwave emissivity, ~ 0.5, so that atmospheric phenomena appear as larger emissions with a good contrast against a low-brightness temperature background. Several factors combine to make retrieval of these same atmospheric parameters much more complicated over land. The land surface emissivities are usually close to unity in densely vegetated areas, making atmospheric features much more difficult to identify against a higher-brightness temperature background. Modulated by vegetation, topography, flooding, and snow, among other factors, the land surface emissivities are not only variable in space and time but are also very complex to model. Until recently, no estimates of the microwave land emissivities over the globe were available at a spatial resolution compatible with the satellite observations. Thus, retrieval of atmospheric properties from microwave, unaided by other information, is problematic.

Since 1987, the Special Sensor Microwave/Imager (SSM/I) instrument on the Defense Meteorological Satellite Program (DMSP) polar satellites senses atmospheric and surface emissions at 19.35, 22.235, 37.0, and 85.5 GHz (Hollinger *et al.* 1987, 1990) with an enhanced sensitivity to clouds compared to previous microwave instruments. The use of SSM/I observations for atmospheric studies over land has been largely restricted to the detection of precipitation. In convective cells, precipitation sized particles can scatter the 85 GHz radiation causing depression of the 85 GHz brightness temperature. Several precipitation algorithms are based on the analysis of these scattering signatures (see the review by Barrett and Kniveton 1995). A few efforts have been directed toward the estimation of cloud liquid water path over land: the work by Jones and Vonder Haar (1990) and its recent development by Greenwald *et al.* (1997) provide the most extensive studies available today on this subject. Before retrieving the cloud liquid water content, they estimate the surface emissivity with the help of collocated visible and infrared satellite observations to determine clear-sky conditions before analysing

* Corresponding author: Columbia University, NASA Goddard Institute for Space Studies, New York, NY 10025, USA.

cloudy scenes. Results are presented for only a few cases. To our knowledge, there has been no attempt to retrieve column water vapour amount over land with SSM/I observations. Although Njoku (1995) concluded from simulations that land surface temperature could be retrieved from multichannel microwave observations with an accuracy of 2 to 2.5 K, few studies have examined this potential. MacFarland *et al.* (1990) investigated the correlation between SSM/I observations and surface air temperature and concluded that 85 or 22 GHz measurements, depending on the surface type, are the most sensitive to the land surface temperature. Since these two frequencies are also the most sensitive to water vapour, this result probably indicates that what is being sensed is perhaps the lower atmosphere rather than the surface. More recently, Basist *et al.* (1998) also proposed a method to retrieve near-surface air temperatures from SSM/I.

Microwave land surface emissivities over the whole globe have recently been estimated from SSM/I observations, by removing the contributions of the atmosphere, clouds and rain using ancillary satellite data (Prigent *et al.* 1997b, 1998). The correspondences between the geographical patterns and seasonal variations of the estimated microwave emissivities are compatible with variations of large-scale topography, vegetation type, flooding and snow cover extent. The standard deviation of the day-to-day variations of the retrieved emissivities within a month are typically about 0.012 for all the SSM/I frequencies, which is a measure of the precision (but not absolute accuracy) of these estimates. Given that these emissivity estimates appear stable over short time periods, we examine the potential and limitations of microwave observations for retrieving surface and atmospheric parameters (surface temperature T_s, integrated water vapour *WV*, and cloud liquid water path *LWP*) over land with SSM/I observations. The detection of rain events will also be discussed.

A sensitivity analysis is conducted to better understand the relationship between the relevant parameters, to assess the limitations of the SSM/I frequencies in sensing the atmosphere over land, and to help select an adequate retrieval method (section 2). In section 3, a variational inversion method is presented, with emphasis on the a priori information derived from the National Centers for Environmental Prediction (NCEP) analysis and from the International Satellite Cloud Climatology Project (ISCCP) data. In section 4, the inversion results are presented and discussed. We specially focus on the analysis of the retrieval errors in order to better understand the information content of the SSM/I observations with respect to the parameters to be retrieved: these quantitative error estimates define under what conditions useful atmospheric and surface information can be derived from SSM/I measurements. Finally, section 5 concludes this study and outlines the potential prospects of this analysis method.

2. Sensitivity analysis

The microwave land surface emissivities show very distinctive geographical patterns related to vegetation, topography and other surface characteristics, with values at horizontal polarization ranging from close to one for densely vegetated areas to 0.8 over deserts. As we show, a very important conclusion is that the sensitivity of the SSM/I observations to the atmospheric parameters (*WV* and *LWP*) and to T_s varies depending on the emissivity of the underlying surface. The radiative-transfer equation is briefly discussed, before analysing the sensitivity of the SSM/I brightness temperatures (T_b) to the geophysical parameters. The sensitivity analysis will be limited to the retrieval of *WV*, *LWP* and T_s. The sensitivity of the SSM/I frequencies to the water vapour vertical structure and to the temperature profile of the atmosphere, already very low over ocean, is expected to be even lower over land and will not be examined in this study.

Over a flat surface, radiative transfer in a non-scattering plane-parallel atmosphere can be expressed in terms of brightness temperature for each orthogonal polarization, suffix p (p stands for either horizontal, H, or vertical, V):

$$T_{bp} = T_s \times \epsilon_p \times e^{-\tau(0,h)\sec\theta} + T_a\downarrow \times (1-\epsilon_p) \times e^{-\tau(0,h)\sec\theta} + T_a\uparrow, \qquad (1)$$

with $T_a\downarrow = \int_0^h T(z)\alpha(z)\sec\theta\, e^{-\tau(0,z)\sec\theta}\, dz$ and $T_a\uparrow = \int_0^h T(z)\alpha(z)\sec\theta\, e^{-\tau(z,h)\sec\theta}\, dz$. T_{bp} is the brightness temperature measured by the satellite for polarization p, T_s is the surface 'skin' temperature, ϵ_p is the surface emissivity for polarization p, θ is the incident angle at the surface, $\alpha(z)$ is the atmospheric absorption by gases and non-precipitating cloud particles at altitude z, $T(z)$ is the atmospheric temperature at altitude z, $\tau(z_0, z_1) = \int_{z_0}^{z_1} \alpha(z)\, dz$ is the atmospheric opacity from z_0 to z_1, and h is the altitude of the satellite.

From (1), assuming no dependence of the surface emissivity on T_s, the T_b sensitivity to T_s is simply $dT_{bp}/dT_s = \epsilon_p \times e^{-\tau(0,h)\sec\theta}$. The atmospheric transmittance $e^{-\tau(0,h)\sec\theta}$ is plotted in Fig. 1 for three different cloud conditions for the SSM/I channels with a 53° observation angle. Even in the presence of optically very thick clouds (*LWP* of 0.5 kg m^{-2}) in a tropical atmosphere, the 19 GHz frequency still shows a large transmittance (>0.75). As a consequence, the sensitivity of this frequency to changes in surface temperature can be as high as 1 K K^{-1} and is not expected to be lower than 0.6 K K^{-1} in rain-free areas. Except for 85 GHz, which is strongly affected by both *WV* and *LWP*, the SSM/I frequencies exhibit a significant sensitivity to surface temperature, even over low-emissivity land surfaces (for a tropical atmosphere with a *LWP* of 0.5 kg m^{-2} and a surface emissivity of 0.8, the sensitivity at 22 GHz is 0.4 K K^{-1}). In the presence of rain, not only will the atmospheric transmittance be reduced but also the surface emissivities may be decreased by surface wetness, making it difficult to retrieve T_s under these conditions (see discussion in section 4). Moreover, while the assumption that ϵ_p is not dependent on T_s is valid for soils (Ulaby *et al.* 1986), it is no longer true for wet surfaces because of the temperature dependence of the water emissivity and, as a consequence, the T_b sensitivity to T_s is even lower in wet regions.

The sensitivity to surface emissivity errors $dT_s/d\epsilon_p$ is $(T_a\downarrow - T_s)/\epsilon_p$. For 19 GHz, where the atmospheric contribution is small, the error dT_s is roughly equal to $-T_s \times d\epsilon_p/\epsilon_p$, meaning that an error of the order of 0.003 in the emissivity induces ~1 K error in the land T_s, for a surface emissivity close to 1.

Figure 2 illustrates the sensitivity of the SSM/I observations to changes in the water vapour column *WV*. The higher the surface emissivity, the lower the sensitivity to *WV* for typical atmospheric conditions. The 22 and 85 GHz channels are the most sensitive to water vapour, but for high surface emissivities (>0.9), the sensitivity of T_b to *WV* does not exceed 0.5 K per kg m^{-2}. As a consequence, one cannot expect an accurate retrieval of the water vapour content from SSM/I over vegetated areas where emissivities are >0.90 for both H and V polarizations. When land emissivities are lower, for example over the desert for the H polarization, the sensitivity of the 22 and 85 GHz channel to *WV* is higher.

For *LWP* the sensitivity of the SSM/I T_b increases with increasing frequency but varies with cloud temperature and surface emissivity (Fig. 3). Over a surface with an emissivity close to one, it is easier to detect higher (i.e. colder) clouds than lower (i.e. warmer) clouds (provided that the cold clouds are not composed of small ice crystals that are not detectable at SSM/I frequencies), while the opposite situation prevails for low surface emissivities. The ability to estimate *LWP* depends essentially on the contrast between the radiance emitted by the cloud and the radiance that emanates from

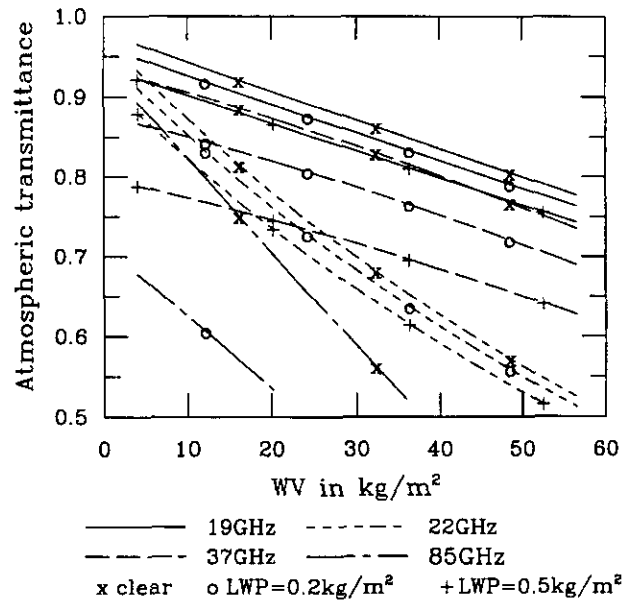

Figure 1. The atmospheric transmittance for the SSM/I observations. The simulations are presented for a tropical atmospheric profile and a surface temperature of 299 K. The water vapour content of the tropical atmosphere is scaled to fit the given water vapour content. Three cloud conditions are presented: Clear sky (×); a 0.2 kg m^{-2} cloud located between 800 and 725 mb with a 273 K mean temperature (○); and a 0.5 kg m^{-2} cloud at the same altitude and temperature (+).

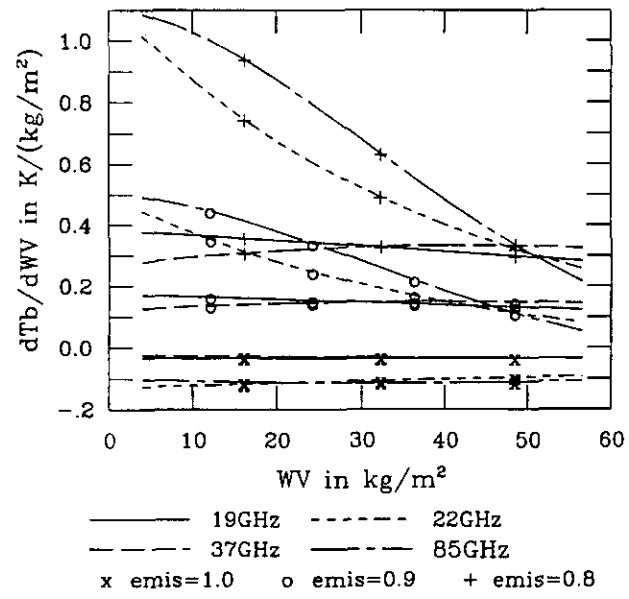

Figure 2. Sensitivity of the SSM/I observations T_b to changes in water vapour (*WV*, K per kg m^{-2}). The simulations are presented for a tropical atmospheric profile and a surface temperature of 299 K. The water vapour content of the tropical atmosphere is scaled to fit the given water vapour content. Three surface emissivities are selected: 1.0 (×); 0.9 (○); 0.8 (+).

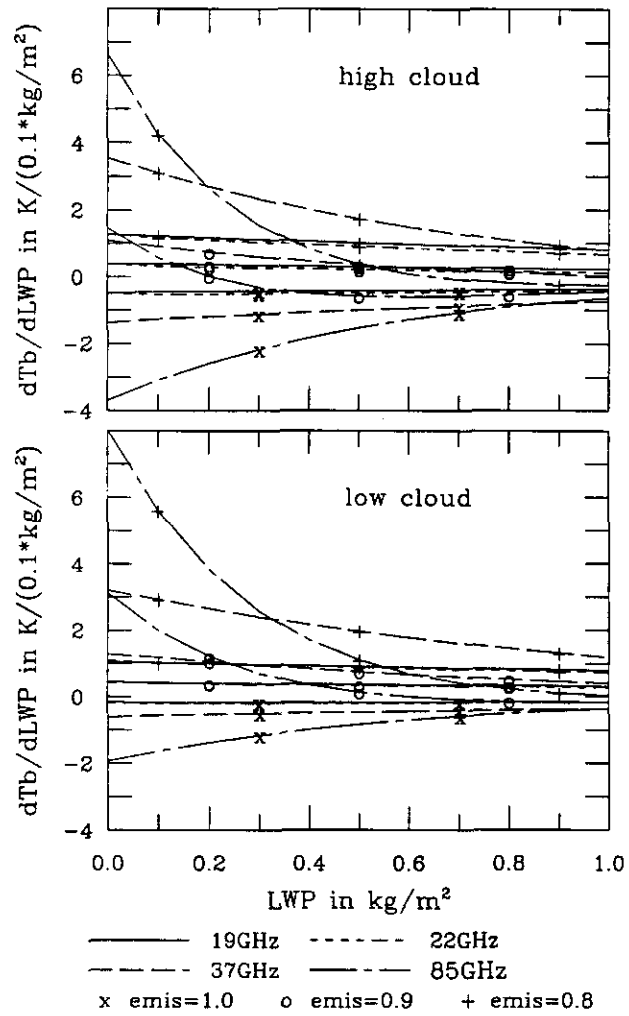

Figure 3. Sensitivity of the SSM/I observations T_b to changes in liquid water path (*LWP*, K per 0.1 kg m^{-2}). The simulations are presented for a tropical atmospheric profile and a surface temperature of 299 K, for a low cloud between 800 and 725 mb with mean temperature 273 K, and for a high cloud between 650 and 585 mb with mean temperature 262 K. Three surface emissivities are selected: 1.0 (×); 0.9 (○); 0.8 (+).

the surface. As a result, the accuracy of a potential *LWP* retrieval will vary with the cloud and surface conditions. The 85 GHz channel exhibits higher sensitivity to *LWP*, especially for low liquid water content but has a very nonlinear behaviour. The 37 GHz channel, although less sensitive, shows a more linear behaviour.

In the selection of a retrieval method, two points have to be considered.

(i) The sensitivity of the SSM/I observations to the parameters we want to estimate is rather low (especially for *WV* and to a lesser extent for *LWP*). The SSM/I radiances also vary with several other parameters (the cloud-top temperature for instance). Several combinations of the parameters to be determined may be consistent with the measurements, unless additional information is added.

(ii) The relationship between the SSM/I observations and the parameters to be retrieved involves nonlinearities, especially at 85 GHz in cloudy situations.

As a consequence, a nonlinear variational retrieval method is proposed to combine different sources of information optimally (namely the SSM/I observations and a priori knowledge of the meteorological situation derived from meteorological analysis and from visible and IR satellite observations), and to handle the nonlinearities of the problem properly. With such a method, it is possible to characterize the estimation error for each retrieved parameter, which gives a framework in which to judge the results and to better assess the information content of the SSM/I observations concerning this parameter. A similar variational retrieval over the ocean has been used at the European Centre for Medium-Range Weather Forecasts (ECMWF) routinely and in real-time since February 1998 to retrieve surface wind speed, *WV* and *LWP* (Phalippou 1996). This method has also been tested against accurate in situ measurements in the framework of the Atlantic Stratocumulus Transition Experiment campaign over ocean (Prigent *et al.* 1997a).

3. A CONSTRAINED VARIATIONAL INVERSION METHOD BASED ON RADIATIVE-TRANSFER CALCULATIONS AND TIED TO A REALISTIC FIRST GUESS

(*a*) *Theory*

The scheme performs a nonlinear inversion of the 7-channel SSM/I measurements, to retrieve simultaneous estimates of T_s, *WV* and *LWP*. It is derived from the Newtonian nonlinear iterative method described by Rodgers (1976) and by Eyre (1989). The unified notation of Ide *et al.* (1997) is used throughout the paper. Let $\mathbf{x}$ be the three-dimensional (3-D) vector representing the geophysical variables to be estimated; $\mathbf{x}^b$ the 3-D vector describing the first-guess geophysical state with $\mathbf{B}$ being the 3×3 error covariance matrix associated to this first-guess; $\mathbf{y}^o$ the 7-D vector of the measured SSM/I brightness temperatures with $\mathbf{E}$ the 7×7 matrix representing the SSM/I observation error covariances; $\mathbf{y}(\mathbf{x})$ the 7-D vector of SSM/I brightness temperatures simulated with a radiative-transfer model for the atmospheric state $\mathbf{x}$ and the 7×7 matrix $\mathbf{F}$ representing the radiative-transfer model errors. Assuming that the errors in the observations and in the a priori information are unbiased, uncorrelated, and have Gaussian distributions, the best estimate of $\mathbf{x}$ will minimize the following function:

$$\chi^2(\mathbf{x}) = J^o + J^b = 1/2\{\mathbf{y}(\mathbf{x}) - \mathbf{y}^o\}^T(\mathbf{E}+\mathbf{F})^{-1}\{\mathbf{y}(\mathbf{x}) - \mathbf{y}^o\} + 1/2(\mathbf{x}-\mathbf{x}^b)^T\mathbf{B}^{-1}(\mathbf{x}-\mathbf{x}^b), \quad (2)$$

where the term J^o in this equation is related to the SSM/I observations (the observation cost function) and the term J^b represents the information related to the initial geophysical state (the background cost function). Superscripts T and -1 correspond to the matrix transpose and inverse, respectively. To find the maximum-probability solution of $\mathbf{x}$, (2) is minimized, i.e. assuming there are no multiple minima, the gradient of $\chi^2(\mathbf{x})$ with respect to $\mathbf{x}$ is set to zero:

$$0 = \mathbf{H}(\mathbf{x})^T(\mathbf{E}+\mathbf{F})^{-1}\{\mathbf{y}(\mathbf{x}) - \mathbf{y}^o\} + \mathbf{B}^{-1}(\mathbf{x}-\mathbf{x}^b), \quad (3)$$

with $\mathbf{H}(\mathbf{x})$ containing the partial derivative of $\mathbf{y}(\mathbf{x})$ with respect to the elements of $\mathbf{x}$. Then, the Newtonian method consists of expanding the brightness temperature vector $\mathbf{y}$ as a Taylor series about a guessed value $\mathbf{x}_n$:

$$\mathbf{y}(\mathbf{x}) = \mathbf{y}(\mathbf{x}_n) + \mathbf{H}(\mathbf{x}_n)(\mathbf{x}-\mathbf{x}_n), \quad (4)$$

yielding:

$$\mathbf{x}_{n+1} = \mathbf{x}_n - \{\mathbf{B}^{-1} + \mathbf{H}(\mathbf{x}_n)^T(\mathbf{E}+\mathbf{F})^{-1}\mathbf{H}(\mathbf{x}_n)\}^{-1} \times [\mathbf{H}(\mathbf{x}_n)^T(\mathbf{E}+\mathbf{F})^{-1}\{\mathbf{y}(\mathbf{x}_n) - \mathbf{y}^o\} + \mathbf{B}^{-1}(\mathbf{x}_n - \mathbf{x}^b)]. \quad (5)$$

The error covariance of the nth guess is given by:

$$\mathbf{A}(\mathbf{x}_n) = \{\mathbf{B}^{-1} + \mathbf{H}(\mathbf{x}_n)^T(\mathbf{E}+\mathbf{F})^{-1}\mathbf{H}(\mathbf{x}_n)\}^{-1}. \quad (6)$$

$\mathbf{A}(\mathbf{x}_n)$ is an estimate of the error covariance of the solution for the step n (Rodgers 1976). For the final vector $\mathbf{x}$ and the corresponding $\mathbf{H}(\mathbf{x})$, the matrix $\mathbf{A}$ is an estimate of the error covariance of the retrieval. It is not a measure of the absolute accuracy of the retrieval, but indicates the ability to reproduce the observed values of T_b with the simulations and, assuming the radiative-transfer model is correct, it is a measure of the retrieval relative accuracy. Within the iterative process, the geophysical variables to be retrieved are constrained to physically meaningful values (essentially they should not turn negative). The NAG procedure E04LBF* has been adopted here: it is based on the Newtonian method and is suitable for finding the minimum of a function with variables subject to fixed bounds (Phalippou 1996).

(*b*) *The radiative-transfer model and its associated errors*

Within the inversion procedure, the radiative-transfer model has to be accurate enough to give a good estimate of the brightness temperatures (see (1)) and their first derivatives with respect to all the geophysical parameters to be retrieved and for all the frequencies. The MPM 93 gaseous-absorption model of Liebe *et al.* (1993) is adopted for all the SSM/I frequencies. In this model, H_2O and O_2 lines are added up to 1 THz, assuming a Van Vleck Weisskopf line shape. For oxygen, this function is modified by Rosenkranz (1992) to include line coupling in the 60 GHz band. An empirical H_2O continuum is added, derived from laboratory measurements (Liebe *et al.* 1993).

Cloud absorption is calculated using the Rayleigh approximation which is valid for most non-precipitating liquid water clouds at SSM/I frequencies. The cloud temperature is assumed to be equal to the air temperature at the same level. The dielectric properties of liquid water are taken from Manabe *et al.* (1987). Scattering by large particles is not considered within the inversion process, but scattering signatures at 85 GHz will be briefly discussed in section 4(c).

The monthly mean microwave emissivities (at each local time of satellite overpass) previously estimated (Prigent *et al.* 1997b) are used in (1) to characterize the surface emission. The standard deviations of day-to-day variations of the retrieval emissivities within a month, σ_ϵ, have been calculated for each channel and for each location. These values are used as an indicator of the accuracy of these estimates. Possible gross errors in the estimated emissivity (due for instance to recent rain or snow events) are not accounted for and will have to be removed by quality control (see the case of a rain event in section 4(a)).

The radiative-transfer error matrix ($\mathbf{F}$ in (2)) should not only include the model errors but also the potential contributions of phenomena that are not accounted for in the radiative transfer (multi-layer clouds, inhomogeneities in the receiver field-of-view, among others). It is not easy to evaluate this matrix objectively, but the main contribution is likely to arise from the estimates of surface emissivity. For an initial atmospheric state $\mathbf{x}^b$, for each location and for each SSM/I channel, the brightness temperature error

* Nag Fortran Library Manual (1991) mark 15, NAG Ltd., Oxford, UK.

dT_b that would result from an emissivity error σ_ϵ is calculated from (1). The errors are supposed to be uncorrelated between channels, leading to a diagonal **F** matrix with the square of dT_b as its diagonal elements. Typical values of dT_b range from 2 to 4 K, depending on the frequency and the atmospheric situation.

(*c*) *The observation errors*

The SSM/I data from the F10 satellite of the DMSP have been obtained from Remote Sensing Systems (Wentz 1988). The radiometric sensitivities of the SSM/I channels have been estimated by Hollinger *et al.* (1990) for the instrument on the F8 satellite, but the F10 radiometers are expected to have similar characteristics. The radiometric noise has a typical value of 0.6 K. The observation noise covariance matrix (**E** in (2)) is assumed to be uncorrelated between channels, so that the off-diagonal elements are zero. The diagonal terms of the matrix are set to the variance of radiometric error of the SSM/I instrument (i.e. the square of 0.6 K).

(*d*) *The first-guess fields and related background errors*

(i) *The water vapour initial fields derived from the National Centers for Environmental Prediction (NCEP) reanalysis.* The inversion method adopted here makes use of prior knowledge of the atmospheric state provided by a meteorological analysis. The first-guess atmospheric profiles used in the inversion process are extracted from the NCEP reanalysis dataset (Kalnay *et al.* 1996): temperatures and relative humidities for eight levels up to 300 mb (middle and lower troposphere). These fields are available every six hours, at a spatial resolution of 2.5° latitude and longitude. For each location, the atmospheric profile has been adjusted for consistency with the topography (i.e. truncation or downward extrapolation of the atmospheric profiles depending on the topography differences between the NCEP reference elevation and ours).

During the inversion process, for each SSM/I pixel, the initial water vapour profile is modified iteratively until minimization of (2) is satisfactory. The water vapour density in each layer of the initial NCEP profile is uniformly scaled, to give the integrated water vapour content imposed during the inversion process. But during the minimization process, the humidity at each atmospheric level should not be supersaturated. Relative humidity in each layer is limited to 100%, and is compensated for by adding water vapour in adjacent layers. For the retrieved variables, the matrix **B** contains the error covariance associated with the a priori information. For each NCEP atmospheric profile, the error is set to 0.4 times the integrated *WV* of the first-guess profile. Very similar *WV* error covariance values are derived when using the error covariance of each humidity level as given by Eyre *et al.* (1993) for the Tiros Operational Vertical Sounder (TOVS) processing. Thus, the microwave determination of *WV* will be judged of value only if it can reduce the uncertainty to less than 0.4 times the mean value.

(ii) *The use of the International Satellite Cloud Climatology Project (ISCCP) dataset.* In the ISCCP data, cloud parameters and related quantities are retrieved from visible (VIS ~0.6 μm wavelength) and infrared (IR ~11 μm wavelength) radiances provided by the set of polar and geostationary meteorological satellites (Rossow and Schiffer 1991). The ISCCP dataset is used in this study to discriminate between clear and cloudy scenes and to give an estimate of the cloud top temperature and of the surface skin temperature. The pixel level dataset (the DX dataset) is selected for its spatial sampling of about 30 km and its sampling interval of 3 hours (Rossow *et al.* 1996).

(I) The surface temperature first-guess: ISCCP provides the surface skin temperature first-guess ($\mathbf{x}^b(1)$ in (2)) retrieved from IR radiances, assuming that the IR emissivity of the surface is 1. Rapid changes of the surface temperature can be observed, for example up to 30 K over the north African desert in 3 hours. Instead of selecting the closest-in-time DX image to derive the surface temperature, a linear interpolation is calculated between two ISCCP surface temperature estimates to the precise time of the SSM/I overpass. If the ISCCP DX scenes are cloudy, a clear-sky compositing procedure is conducted within the ISCCP process to derive an estimation of the surface temperature (see Rossow and Garder 1993b for more details). In the matrix **B**, the error associated to the surface temperature is fixed at 4 K. This value corresponds to the estimated error in the ISCCP skin temperature (Rossow and Garder 1993a,b).

(II) The cloud first-guess: First the ISCCP data helps discriminate between clear and cloudy scenes. Over the ocean, it has been shown that the VIS and IR observations have a better ability to detect clouds than the microwave measurements (Lin and Rossow 1994). Given that the sensitivity of the microwave to clouds over land is lower than over ocean, when a pixel is considered clear by the ISCCP procedure, the *LWP* is fixed to zero in our inversion process and is not modified during the inversion process ($\mathbf{x}(3)$ and $\mathbf{x}^b(3)$ are fixed to zero). The sensitivity of the microwave for detecting clear scenes will be discussed further in section 4(c).

For cloudy scenes, the determination of the cloud vertical structure combines information from the ISCCP analysis and the NCEP atmospheric profile. Lin and Rossow (1994) have indicated the effect of cloud temperature on *LWP* retrieval over ocean. Wang and Rossow (1995) and Wang (1996) have shown that rawinsonde observations can provide an estimate of the cloud vertical structure, including cloud top and cloud base heights and the characteristics of multi-layered clouds. Unfortunately, such observations are not available with good enough space–time coverage and resolution, so we use the NCEP humidity profile (cf. Sheu *et al.* 1997). In this feasibility study, multi-layer clouds and fractional cloud cover are not considered. The vertical location of the cloud top is derived from the DX pixel cloud top temperature information collocated to within 1.5 hour and ~30 km. The initial NCEP 8-level profile up to 300 mb is subdivided into 18 levels for a more accurate definition of the cloud layers.

If the DX cloud top temperature is $\geqslant$260 K, it is assumed that the cloud is composed mainly of liquid water (cf. Lin and Rossow 1997) and the location of the cloud top layer is dictated by the ISCCP cloud top temperature.

If the ISCCP cloud top temperature is <260 K, the higher portion of the cloud is probably formed of ice, and the contribution of the ice in the cloud is not considered. Because of the possibility that this ice cloud obscures a liquid cloud or becomes a liquid cloud below, a possible liquid water cloud layer is located either from the 24 closest DX pixels or from the NCEP humidity profile. If any neighbouring pixels are cloudy with cloud top temperatures over 260 K, the average cloud top temperature is used. If this is not the case, the NCEP humidity profiles are analysed as follows. A cloudiness likelihood parameter is defined for each atmospheric layer, $lc = (rh - rhc)/(100\% - rhc)$, which compares the relative humidity of the layer, rh, to the relative humidity, rhc, for which there is a good probability of having a cloud (see Sheu *et al.* (1997) who use the same parameters based on the work of Slingo (1987)). To derive rhc the ISCCP data is correlated with the NCEP water vapour profiles. For a month, for each 2.5° in latitude and longitude, the relative humidity in the NCEP reanalysis profile is associated with a cloud top level in coincident ISCCP pixels (see Sheu *et al.* 1997 for a similar development). For each 2.5° cell within the studied area, rhc has been calculated at

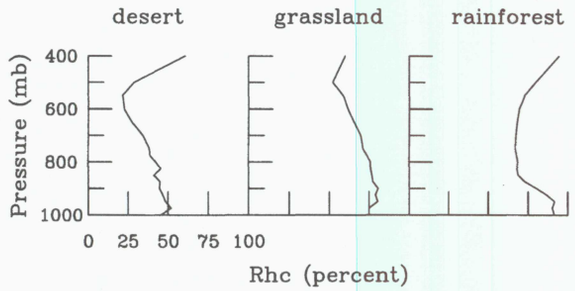

Figure 4. Most probable relative humidity *Rhc* in the atmospheric layers when clouds are present for three locations over different surface types (desert, grassland, and rain forest). The results are derived from the National Centers for Environmental Prediction relative humidity profiles coincident with the ISCCP (see text) cloud-top estimates. The results are averaged over October 1991.

each level corresponding to an ISCCP cloud top. The *rhc* parameter is dependent on the geographic location: Fig. 4 represents the *rhc* profiles for three different locations. For DX cloud top temperatures <260 K, the liquid cloud top corresponds to the highest atmospheric layer with $T \geqslant 260$ K and $lc \geqslant 0$.

Given a cloud top temperature, the NCEP humidity profile is further examined to derive the vertical extent of the cloud. The cloud base corresponds to the atmospheric layer for which $lc < 0$. Within the cloud, the *LWP* is scaled with respect to the lc parameter for each atmospheric layer. The initial *LWP* $\mathbf{x}^b(3)$ is set to the average cloud liquid water path estimated from ISCCP optical thickness for the month (in the ISCCP D2 data set; Rossow *et al.* 1996). The background error on the *LWP* is arbitrary, set to 3 kg m^{-2} in the **B** matrix which means that the *LWP* inversion is actually not constrained by the first guess: the microwave measurements must then provide any information on *LWP*.

4. Results and Discussion

Our analysis method is applied to F10 DMSP SSM/I data within the Meteosat area from October 10 to October 18 1991, for daytime observations (to allow a comparison with the ISCCP *LWP* estimates). For October 11 further sensitivity tests have been performed and the retrieved fields are presented. In Fig. 5, the SSM/I daytime values of T_b show that, contrary to ocean situations, cloud structures are not easy to identify since the SSM/I observations are the result of a complex combination of surface and atmospheric contributions. The brightness temperatures have been calculated for the first-guess solution (using ISCCP T_s and the NCEP atmospheric profile) without any cloud. The difference between the observed SSM/I values of T_b and the cloud-free simulated values of T_b are also presented on Fig. 5. Even with most of the background complexity removed, it is still difficult to identify cloud structures; the range of variation of the differences is small, usually <10 K. A warm feature at one frequency can appear as a cold feature at another frequency; over the Sahara for instance, a large cloud structure with low cloud-top temperatures (as estimated by ISCCP) appears mostly as a warm feature at 37 GHz (on Fig. 5, the brightness temperature difference is higher than in the surrounding area), while this is not the case at 85 GHz. The same is true in different regions over France. On the other hand, a warm cloud-top structure north of Somali has a weak signature at 37 GHz but a much warmer counterpart at 85 GHz.

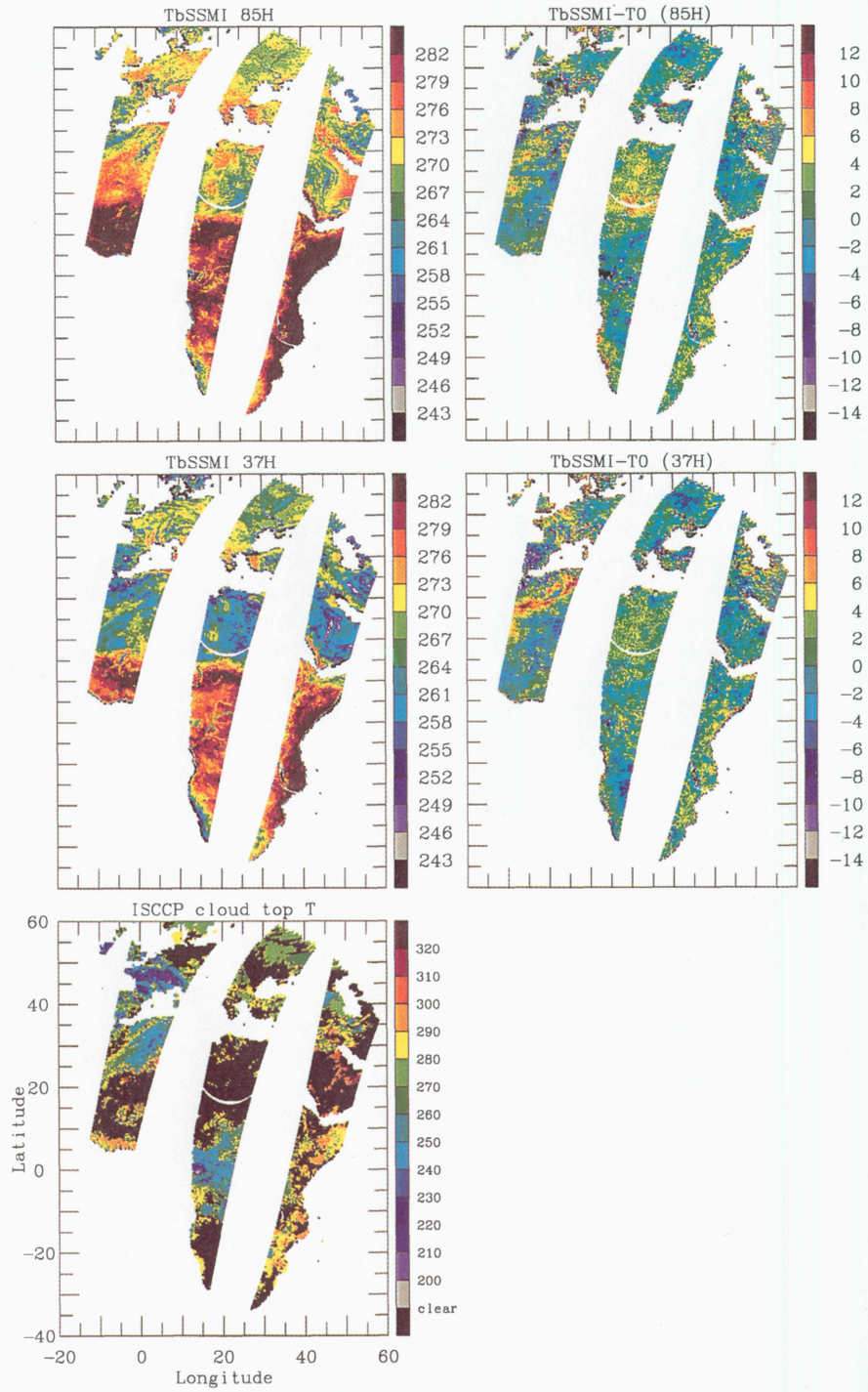

Figure 5. The SSM/I observed brightness temperatures (T_b SSMI, morning orbits) for 11 October 1991, in the Meteosat area, along with the difference between the SSM/I observations and the simulations corresponding to cloud-free first-guess atmospheric states (T_b SSMI-T_o). Results are presented at 37 and 85 GHz for horizontal polarizations. The ISCCP (see text) cloud-top temperatures (T) are also presented for the same situation.

TABLE 1. OBSERVED MINUS COMPUTED T_b STATISTICS AT THE END OF THE INVERSION PROCESS (187573 PIXELS)

Channel	Mean (K)	Standard deviation (K)
19 GHz V	−.28	1.93
19 GHz H	.07	3.14
22 GHz V	−.14	1.25
37 GHz V	−.06	1.51
37 GHz H	.00	2.86
85 GHz V	.11	1.25
85 GHz H	.13	1.75

In the following statistical analysis, most results are discussed separately for three ranges of surface microwave emissivities and for clear and cloudy scenes, since different sensitivities to the retrieved parameters are expected depending on the surface and cloud characteristics. The surface types are classified according to the emissivity of the surface at 19 GHz in the H polarization, which is crudely related to the vegetation density (cf. Prigent *et al.* 1997b). Surfaces with 19 GHz emissivity <0.9 for the H polarization generally correspond to desert-like areas; zones of dense vegetation show 19 GHz emissivities >0.95 (see Plates 1 and 3 in Prigent *et al.* 1997b). Cloudy scenes are divided into two groups according to their *LWP* estimated by ISCCP (cf. Lin and Rossow 1994). Cloudy scenes with cloud-top temperatures <260 K have been excluded from this analysis, because these clouds are likely to be at least partly formed of ice and the ISCCP *LWP* values may not be representative of the actual liquid water path.

The inversion procedure has been tested for different configurations: when using all 7 SSM/I channels but also when using only the 5 lower frequency channels. This test helps to determine the impact of the 85 GHz channel on the retrieval, namely to quantify the enhanced sensitivity to water vapour and low *LWP* obtained by using the high-frequency channels. In cloud-free areas (as specified by the ISCCP coincident estimate), the inversion procedure is also applied without fixing *LWP* to zero: the dispersion of the corresponding derived *LWP* values will give an estimate of the SSM/I *LWP* retrieval uncertainty.

After the inversion process, and at the end of the minimization, the differences between the observed and computed SSM/I radiances are small for all the channels, lower than the noise assumed in the measurements and in the radiative-transfer model. Table 1 gives the mean values and the standard deviations of these differences for the studied orbits, when applying the inversion procedure to seven channels and fixing the *LWP* to zero when the coincident ISCCP observation is cloud-free. The biases that were observed at the end of the inversion process over ocean (Phalippou 1996; Prigent *et al.* 1997a) do not appear here. As the inversion scheme makes use of the microwave emissivities retrieved with the same SSM/I observations, the biases of the measured brightness temperatures (if there were any) are cancelled out.

(a) *The surface temperature*

For each pixel, the theoretical error in the retrieval is calculated from the **A** matrix in (6) after the inversion procedure; the results for the surface temperature are presented in Fig. 6 for three ranges of surface microwave emissivity and two ranges of *LWP* and clear conditions. These errors indicate a very promising improvement compared with the first-guess errors of 4 K. The SSM/I observations have a real potential to monitor the surface temperature to within 1–2 K, provided that the surface emissivities are estimated

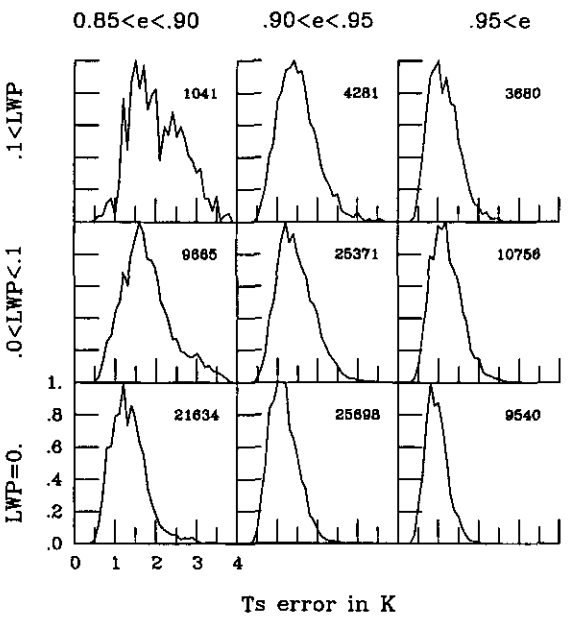

Figure 6. Normalized histograms of the theoretical errors in the surface temperature (T_s) retrieval, calculated when using the 7 SSM/I channels for the SSM/I morning orbits in the Meteosat area from 10 to 18 October 1991. Results are presented for three cloud conditions: clear sky, liquid water path $LWP = 0$; $0 <$ ISCCP $LWP < 0.1$ kg m^{-2} and cloud-top temperature $\geqslant 260$ K; 0.1 kg m$^{-2} <$ ISCCP *LWP* and cloud-top temperature $\geqslant 260$ K. Three ranges of surface emissivity, e, at 19 GHz horizontal polarization are included. The number of SSM/I inverted pixels is given for each category. See text for further details.

previously. The accuracy of the retrieval increases slightly with increasing surface emissivity (because the surface contribution to the observed values of T_b increases) and is not much affected by the presence of clouds, at least over vegetated areas (higher emissivities). For a limited number of orbits, the theoretical accuracy of the retrieval has also been calculated when using only the 5 lower-frequency channels and without the assumption that the *LWP* is zero in clear-sky conditions. Although the 7-channel errors are noticeably smaller than the 5-channel errors (0.3 K increase of the mean error when using only 5 channels), whatever the number of channels used in the retrieval, and whatever the first-guess *LWP* for clear-sky cases, the accuracy of the retrieval is very stable, indicating that the retrieval of surface temperature is robust. This presents an attractive possibility to supplement the infrared (IR) surface temperature estimates. For cloud-free pixels, the ISCCP retrieves the actual surface skin temperatures from the IR observations (there is still a small bias because the surface IR emissivity is not known); but when clouds are present, the surface temperature cannot be directly estimated from IR sensors. A less accurate 'composite' skin surface temperature can be estimated by statistically analysing the estimated surface temperatures before and after the cloud overpass (see Rossow and Garder 1993a,b).

Because of the lack of in situ coincident measurements of the surface skin temperature, the SSM/I T_s estimations are compared to the actual ISCCP surface skin temperature for cloud-free pixels and to the ISCCP 'composite' surface skin temperatures for cloudy pixels. The normalized histograms of the differences between the SSM/I and ISCCP estimates are presented in Fig. 7. The difference dispersion increases from ~2.3 K under clear conditions to ~3.5 K in the presence of thicker clouds. This larger

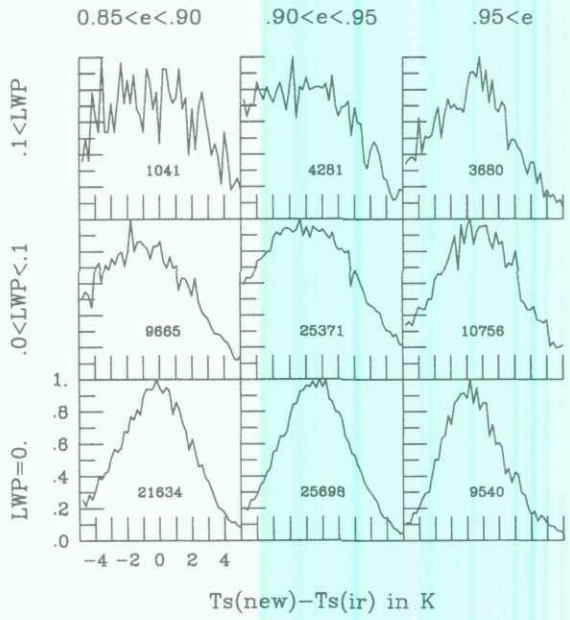

Figure 7. As Fig. 6 but normalized histograms of the differences between the retrieved T_s and the ISCCP *LWP* values.

dispersion can partly be explained by the ISCCP 'composite' surface temperature under cloudy conditions being less accurate. This effect is stronger in areas where the emissivity is low. Figure 8 presents the T_s fields for ISCCP and for our retrieval for 11 October 1991. The global patterns are very similar except over Spain and Morocco, where the retrieved T_s are significantly lower than the ISCCP values (by of the order of 10 K). This special feature has been examined in detail over a few days, with the help of the Meteosat DX images. An optically thick cloud system covers this area, starting on 9 October, probably with related rain events. Figure 9 shows the time series of the ISCCP T_s and cloud-top temperature, along with the NCEP near-surface air temperature, with the SSM/I clear-sky observations, and with the emissivities at 19 GHz V polarization for the area situated around 40°N and 5°W. During the cloud event, the ISCCP does not directly retrieve the surface skin temperature, but instead relies upon the 'compositing' procedure to estimate the surface temperature. In Fig. 9 the decrease in surface air temperature recorded by NCEP after 8 October during the cloudy period is not apparent in the ISCCP estimate until 10 October: because of cloud cover, the ISCCP procedure cannot capture this temperature decrease until after the clouds pass (see Rossow and Garder 1993b). However, this alone cannot account for the large differences between the ISCCP and SSM/I estimates. It is likely that the optically thick cloud system was associated with rain, since the ISCCP cloud-top temperature decreases sharply and the ISCCP *LWP* estimates are high (from 0.2 kg m^{-2} up to 0.7 kg m^{-2}) from 9 October to 13 October (not shown). The IR emissivity is assumed to be 1 in the ISCCP T_s retrieval. Although the real IR emissivity values can vary from place to place from $\sim$ .95 for bare dry soil to 1 in vegetated areas, for a given location their fluctuations with soil moisture are expected to be small and should not affect the ISCCP T_s retrieval. Although it is not possible to estimate microwave surface emissivity when clouds are present, the wet conditions on the surface are likely to induce a decrease of the microwave emissivities that would remain low after the passage of the cloud system (on 14 October). Using the

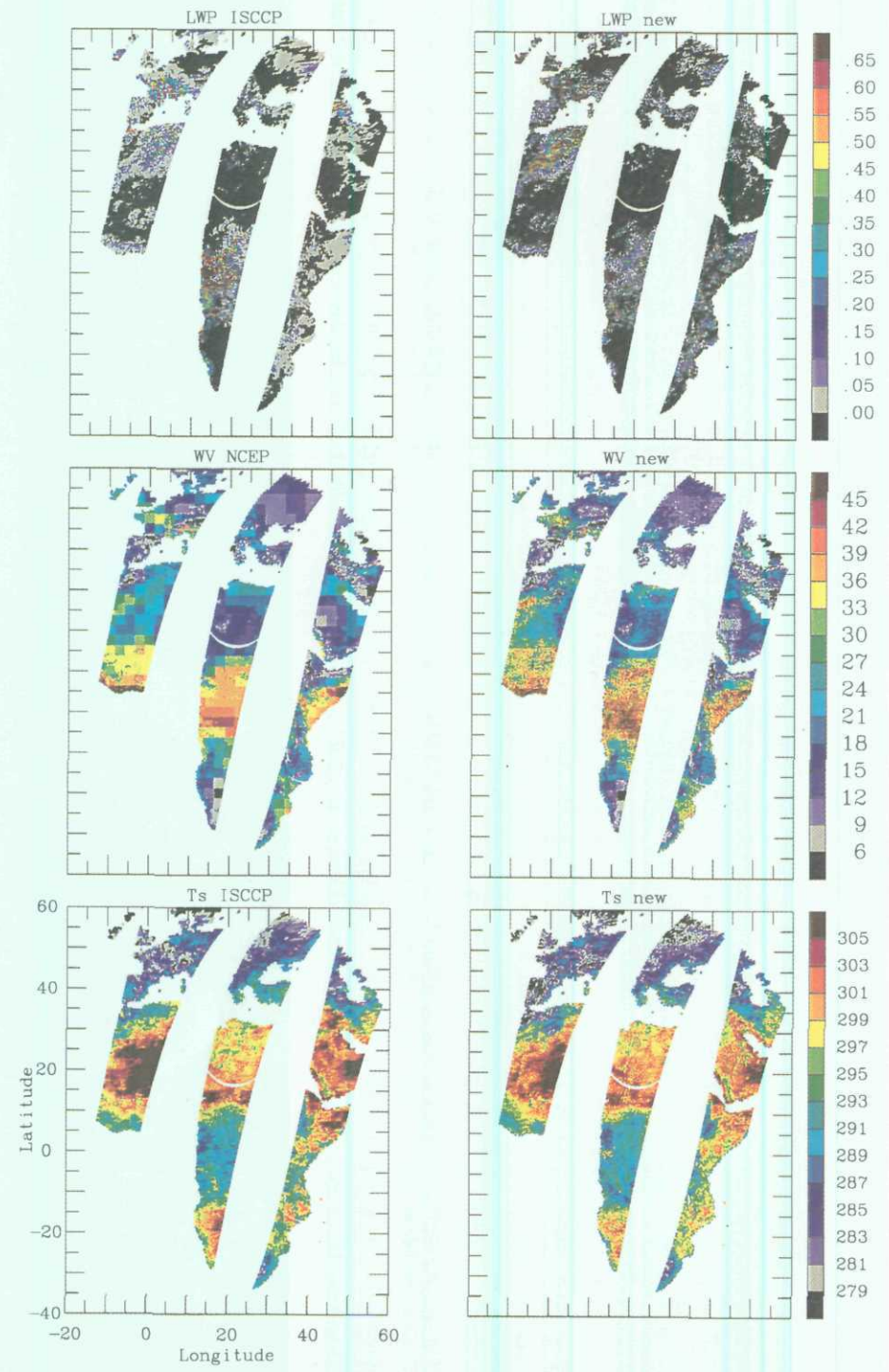

Figure 8. For 11 October 1991, SSM/I morning orbits in the Meteosat region, from bottom to top: ISCCP surface temperature, T_s, and SSM/I retrieved T_s in K; NCEP water vapour, *WV*, and SSM/I retrieved *WV* in kg m^{-2}; ISCCP liquid water path, *LWP*, and SSM/I retrieved *LWP* in kg m^{-2}. See text for further details.

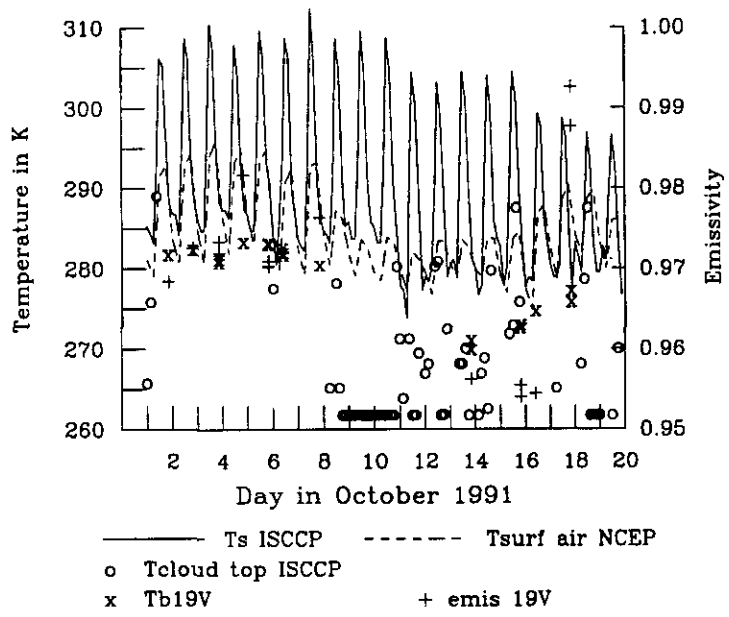

Figure 9. For 40°N and 5°W, time series of the ISCCP surface temperature (T_s, solid line), the NCEP near-surface air temperature ($T_{surf\,air}$, dashed line), and ISCCP cloud-top temperature ($T_{cloud\,top}$, o). The cloud-top temperatures lower than 262 K have been fixed at 262 K for clarity. For cloud-free situations, the SSM/I brightness temperature at 19 GHz vertical polarization (T_b 19V, ×) and surface emissivities at 19 GHz vertical polarization (*emis* 19V, +) are also plotted.

monthly averaged surface emissivity to retrieve T_s with SSM/I, as we do, the retrieved T_s will be underestimated when the actual surface emissivity is temporarily lowered by rain events. For this area on 11 October, the differences between the observed and calculated T_b after the inversion process are exceptionally large at 19 GHz V polarizations (lower than ~ -5 K), suggesting that the retrieval is not correct. As a consequence, although changes in the surface emissivities can have a damaging effect on the T_s retrieval, it may be possible to diagnose these errors related to emissivity variations by examining the difference between the observed and calculated T_b after the retrieval for the channels that are the most sensitive to the surface, i.e. the 19 GHz channels. In particular, as we discuss below, the microwave observations may be useful in detecting precipitation events over land that would aid such diagnosis. Later, when the surface has probably dried out, the retrieved T_s in these areas is again close to the ISCCP estimates.

(*b*) *The water vapour estimation*

The theoretical (relative) accuracy of the *WV* estimation is presented in Fig. 10 as calculated from (6) at the end of the inversion process. The background error associated with the NCEP first-guess has been taken to be 0.4 multiplied by the *WV* first-guess, which corresponds to a relative error of 0.4 (see section 3). Figure 10 shows that the *WV* retrieval is beneficial only in clear-sky conditions. In cloudy situations, the relative errors after inversion do not show a significant improvement over the assumed background errors, meaning that the radiometric observations used in the retrieval do not convey sufficient additional information concerning the *WV*. When using only the five lower-frequency SSM/I channels the results are worse, because of the relatively high sensitivity of the 85 GHz channels to the *WV*. The accuracy of the retrieval increases somewhat with

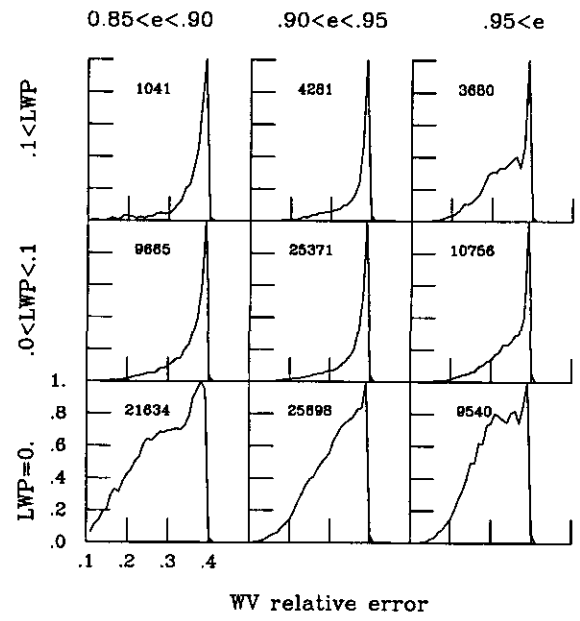

Figure 10. As Fig. 6 but for the water vapour (*WV*) theoretical errors.

decreasing vegetation density (decreasing microwave surface emissivity): in densely vegetated areas, where all the SSM/I channels have a high surface emissivity, the strong surface contribution makes it generally more difficult to detect the water vapour structures. However, for $LWP > 0.1$ kg m^{-2} and surface emissivity > .95, the histogram in Fig. 10 shows a significant population with lower *WV* relative error. These pixels correspond to a large cloud structure in the rain forest area around 0°N and 15°E with cloud-top temperature below 273 K. There is some evidence (Lin and Rossow 1996) that in tropical areas, ice is prevalent in clouds with top temperature up to 273 K, which is not true on a global basis (threshold around 260 K). These pixels in Fig. 10 thus correspond to areas where the *LWP* is, in fact, lower than what ISCCP predicts. In addition, in this rain forest area the surface emissivity is very high (close to 1), and there is a significant amount of *WV* (see Fig. 8). If the water vapour emits at a temperature lower than the surface temperature, it is detectable over this very high emissivity background.

Thus, estimation of the water vapour with SSM/I is generally not useful, except that it could provide an alternative over the desert where rawinsondes are particularly scarce and where the TOVS retrievals show spurious space and time variations (Prigent *et al.* 1997b). Figure 8 compares the SSM/I retrieved *WV* fields on 11 October 1991 with the corresponding NCEP estimations. Although very similar, some of the smaller spatial-scale variations in the SSM/I results appear to be real.

(*c*) *The cloud retrieval*

The theoretical accuracy of the *LWP* retrieval is presented in Fig. 11, separating low and high clouds (low and high clouds correspond, respectively, to ISCCP cloud-top temperatures higher and lower than 260 K). As expected, the accuracy of the retrieval is better for low warm clouds over a radiometrically cold background (low emissivity) and for high cold clouds over a radiometrically warm surface (high emissivity). Nevertheless, whatever the land surface type, with ~0.1 kg m^{-2} error in the *LWP* estimate which

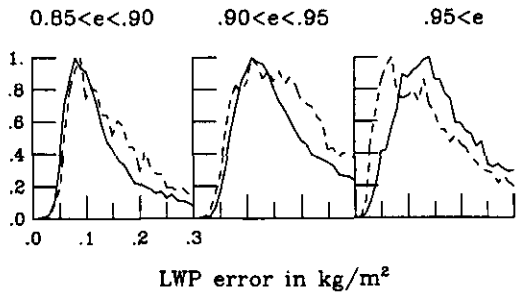

Figure 11. Theoretical accuracy of the liquid water path, *LWP*, retrieval. The results are presented separately for low clouds (ISCCP (see text) cloud-top temperature higher than 260 K, full line) and high clouds (ISCCP cloud-top temperature lower than 260 K, dashed line). Three ranges of surface emissivity, *e*, are included.

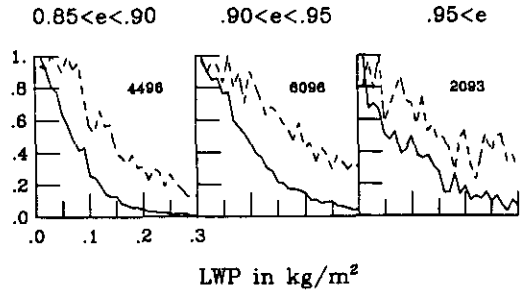

Figure 12. Normalized histograms of the SSM/I liquid water path, *LWP*, retrieved values for ISCCP (see text) clear-sky cases (11 October 1991, SSM/I morning orbits). The results are presented from using the seven SSM/I channels (full lines) and when using only the 5 lower-frequency channels (dashed lines). Three ranges of surface emissivity, *e*, are included, and the number of SSM/I inverted pixels is given for each category.

corresponds to a visible optical thickness of ~15, these results indicate that low-*LWP* clouds will not be accurately measured over land with SSM/I data, even when aided by additional datasets. ISCCP results show that the majority of clouds are optically thinner (Rossow and Schiffer 1991). To further test the sensitivity of the SSM/I observations for low *LWP*, the inversion scheme has been applied to SSM/I pixels coincident with ISCCP clear-sky pixels, without fixing *LWP* to be zero. The dispersion of the SSM/I retrieved *LWP* in clear-sky conditions is ~ 0.1 (Fig. 12). It gives a measure of the accuracy of the retrieval and confirms the theoretical error estimation. Figure 12 also stresses the importance of the 85 GHz channels to the *LWP* retrieval as compared to a retrieval scheme using only the 5 lower-frequency channels.

Figure 8 compares the ISCCP and the SSM/I *LWP* for 11 October (morning orbits). The ISCCP *LWP* has been plotted even when the ISCCP cloud-top temperature was below 260 K, i.e. for areas where the cloud top is mainly composed of ice particles and where the ISCCP *LWP* estimates may not be very reliable. Although the SSM/I *LWP* fields are less smooth ('noisier') than their ISCCP counterparts, the large cloud structures are well captured. Figure 13 presents the distribution of the SSM/I *LWP* minus the ISCCP *LWP* for clouds with ISCCP top temperature greater than 260 K. Whatever the surface type, differences are centred on zero. The left wings of the histograms mainly represent pixels that have been misinterpreted as cloud-free by SSM/I while the ISCCP estimates indicate small *LWP*. The higher the surface emissivity the broader this left wing of the histograms, because the sensitivity of SSM/I to small

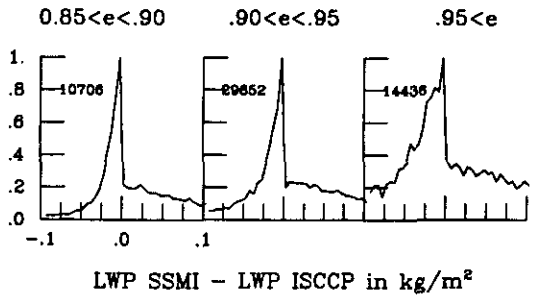

Figure 13. Normalized histograms of the SSM/I liquid water path, *LWP*, minus ISCCP (see text) *LWP*. Only the daytime cloudy pixels are considered with ISCCP cloud-top temperature higher than 260 K. Results are presented for three ranges of surface emissivity, *e*, at 19 GHz horizontal polarization, and the number of SSM/I inverted pixels is given for each category.

LWP decreases with increasing surface emissivity. The right wings of the histograms correspond to overestimation of the SSM/I *LWP* values as compared to ISCCP estimates. Independently of the land surface type, when the pixels are not misclassified by SSM/I as cloud-free the SSM/I *LWP* estimates are generally higher than the ISCCP estimates. The low accuracy of the SSM/I *LWP* may be partly responsible; because *LWP* is constrained to be $\geqslant 0$ in this analysis, the Gaussian error hypothesis is not valid for this variable close to the lower bound ($LWP = 0$) and, as a consequence, the mean *LWP* can be biased high. However the ISCCP *LWP* values are calculated assuming a particle size that is likely to become an underestimate as clouds become progressively denser. For example, Han *et al.* (1994) show a general increase of particle size with increasing optical thickness.

In the SSM/I inversion process, the *LWP* has been retrieved without specific distinction between clouds and rain. Nevertheless, because the SSM/I frequencies are also sensitive to precipitation, it is probable that for higher *LWP*, rain contributes significantly to the total *LWP* (cf. Lin and Rossow 1997). For light precipitation, the small liquid rain drops will not induce much volume scattering, so that the rain contribution will be very similar to that from the cloud, preventing discrimination between rain and cloud. Rain per se is not accounted for separately in the inversion with its own characteristics (drop size distribution and temperature, altitude range, potential scattering of the microwave radiation) and, as a consequence, the inversion process is likely to undergo difficulties in case of heavy precipitation. The observation cost function, J°, at the end of the minimization procedure can be tested as a post-processing criterion to diagnose major rain events.

For 11 October 1991, the areas where J° is greater than 3.5 (i.e. the difference between the observed and simulated T_b are on the average greater than the channel noise) and the areas where SSM/I *LWP* is higher than 0.5 kg m^{-2} have been compared (not shown here). Lin and Rossow (1997) have estimated that over ocean, there is a 50% chance of precipitation from clouds with *LWP* >0.5 kg m^{-2}. The areas with large J° and the clouds with SSM/I *LWP* >0.5 kg m^{-2} show similar patterns. Spencer *et al.* (1989) have shown that the threshold of 255 K for the SSM/I 85 GHz channel discriminates between precipitating and non-precipitating areas, because of the depression of values of the 85 GHz T_b by scattering by large particles. The scattering index (Grody 1991) has also been compared to J°. As expected, the scattering index gives a false signature over the desert, but over France the areas with scattering index larger than 10 correspond fairly well with the regions of large J°. The 255 K threshold on the 85 GHz values of T_b and the large J° indicate rain in similar areas, but the spatial extent of the areas above

the 255 K threshold is much smaller. It is worth noting that for these orbits, the Ferraro *et al.* (1996) method does not predict any rain events. Although no comparisons have been made so far with radar measurements, thresholding the observation cost function as a criterion for rain detection warrants further investigation.

5. Conclusion

The potential to retrieve surface temperature, water vapour content and cloud liquid water path from SSM/I observations over land has been examined using a variational inversion scheme. The method relies upon prior estimates of the monthly mean land surface emissivity, and exploits a priori information on the atmospheric situation as a first-guess and to provide some parameters (ISCCP data and NCEP analysis). The inversion process has been applied to 9 days of daytime SSM/I observations for October 1991 within the Meteosat area. After the inversion process it is possible to calculate the theoretical accuracy of each retrieved parameter, and for this to be used as an efficient quality control. The theoretical accuracy of the T_s retrieval is of the order of 1 K, does not strongly depend on the land surface type (i.e. the surface microwave emissivity), and is not very sensitive to the presence of small-*LWP* clouds. The microwave result can be a reliable alternative when IR observations are blocked by clouds. The SSM/I T_s retrieval has been shown to be sensitive to significant changes in the microwave emissivities (precipitation related soil moisture for example), but these events could be identified with the help of a post-processing stage. The SSM/I sensitivity to *WV* over land is very low except for clear-sky conditions in the most arid areas where the land surface microwave emissivity is smallest. In such areas, estimation of the water vapour with SSM/I could provide an alternative over the desert where the rawinsondes are particularly scarce and where the TOVS retrieval has difficulties. As expected, the accuracy of the *LWP* retrieval depends upon the contrast between the cloud and background radiations, i.e. upon the microwave surface emissivity and cloud temperatures. With an accuracy of ~ 0.1 kg m^{-2}, small-*LWP* clouds are not properly characterized; however, the major cloud structures are well delineated, and qualitative agreement is observed between the ISCCP visible estimates and those of the SSM/I. In addition, SSM/I *LWP* estimates can be derived night and day, which is not possible with the ISCCP estimates. This inversion process also has some ability to detect rain events.

Over the ocean similar variational methods are presently used routinely and in real-time at ECMWF. To avoid excessive computation time, they make use of a fast radiative-transfer model and its adjoint. This computationally efficient process could be adapted to the land cases. An atlas of SSM/I land surface emissivity is presently under development, with a 0.25° spatial resolution. The intra-annual variability of the monthly mean emissivities is analysed to determine the number of emissivity values to be stored per year for an adequate representation of the annual cycle.

Acknowledgements

This work is supported by the NASA Mission to Planet Earth program. We are grateful to A. Walker for her help in processing the ISCCP datasets. We thank the associate editor and one anonymous reviewer for a thorough reading of our paper and for valuable comments. NCAR/NCEP reanalysis data have been provided through the NOAA Climate Diagnostics Center (http://www.cdc.noaa.gov).

References

Barrett, E. C. and Kniveton, D. 1995 Overland precipitation. In *Passive microwave remote sensing of land–atmosphere interaction*. Eds. B. J. Choudhury, Y. H. Kerr, E. G. Njoku and P. Pampaloni. Utrecht, The Netherlands

Basist, A., Grody, N. C., Peterson, T. C. and Williams, C. N. 1998 Using the Special Sensor Microwave/Imager to monitor land surface temperatures, wetness, and snow cover. *J. Appl. Meteorol.*, **37,** 888–911

Eyre, J. R. 1989 Inversion of cloudy satellite sounding radiances by nonlinear optimal estimation. I: Theory and simulation for TOVS. *Q. J. R. Meteorol. Soc.*, **115,** 1001–1037

Eyre, J. R., Kelly, G. A. and McNally, A. P. 1993 Assimilation of TOVS radiance information through one-dimensional variation analysis. *Q. J. R. Meteorol. Soc.*, **119,** 1427–1463

Ferraro, R. R., Weng, F., Grody, N. C. and Batist, A. 1996 An eight-year time series of rainfall, clouds, water vapor, snow cover, and sea ice derived from SSM/I measurements. *Bull. Am. Meteorol. Soc.*, **77,** 891–905

Greenwald, T. J., Combs, C. L., Jones, A. S., Randel, D. L. and Vonder Haar, T. H. 1997 Further developments in estimating cloud liquid water over land using microwave and infrared satellite measurements. *J. Appl. Meteorol.*, **36,** 389–405

Grody, N. C. 1991 Classification of snow cover and precipitation using the Special Sensor Microwave/Imager (SSM/I). *J. Geophys. Res.*, **96,** 7423–7435

Han, Q. Y., Rossow, W. B. and Lacis, A. A. 1994 Near-global survey of effective cloud droplet radii in liquid water clouds using ISCCP data. *J. Climate*, **7,** 465–497

Hollinger, J. P., Lo, R., Poe, G., Savage, R. and Pierce, J. 1987 'Special Sensor Microwave/Imager user's guide'. Available from the Navy Research Laboratory Washington, D.C. USA

Hollinger, J. P., Pierce, J. L. and Poe, G. A. 1990 SSM/I instrument evaluation. *IEEE Trans. Geosc. Remote Sensing*, **28,** 781–790

Ide, K., Courtier, P., Ghil, M. and Lorenc, A. C. 1997 Unified notation for data assimilation: Operational, sequential and variational. *J. Meteorol. Soc. Jpn*, **75,** 181–189

Jones, A. S. and Vonder Haar, H. T. 1990 Passive microwave remote sensing of cloud liquid water over land regions. *J. Geophys. Res.*, **95,** 16673–16683

Kalnay, E., Kanamitsu, M., Kistler, R., Collins, W., Deaven, D., Gandin, L., Iredell, M., Saha, S., White, G., Woolen, J., Zhu, Y., Chelliah, M., Ebisuzaki, W., Higgins, W., Janowiak, J., Mo, K. C., Ropelewski, C., Wang, J., Leetmaa, A., Reynolds, R., Jenne, R. and Joseph, D. 1996 The NCEP/NCAR 40-year reanalysis project. *Bull. Am. Meteorol. Soc.*, **77,** 437–470

Liebe, H. J., Hufford, G. A. and Cotton, M. G. 1993 'Propagation modeling of moist air and suspended water/ice particles at frequencies below 1000 GHz'. Pp. 17–21 in Proceedings of the Specialist meeting of the Electromagnetic Wave Propagation Panel, Advisory Group for Aerospace Research and Development, Palma de Mallorca, Spain

Lin, B. and Rossow, W. B. 1994 Observations of cloud liquid water path over oceans: Optical and microwave remote sensing methods. *J. Geophys. Res.*, **99,** 20907–20927

1996 Seasonal variation of liquid and ice water path in non-precipitating clouds over oceans. *J. Climate*, **9,** 2890–2902

1997 Precipitation water path and rainfall rate estimates over oceans using special sensor microwave imager and International Satellite Cloud Climatology Project data. *J. Geophys. Res.*, **102,** 9359–9374

MacFarland, J. M., Miller, R. L. and Neale, C. M. U. 1990 Land surface temperature derived from the SSM/I passive microwave brightness temperatures. *IEEE Trans. Geosci. Remote Sensing*, **28,** 839–845

Manabe, T., Liebe, H. J. and Hufford, G. A. 1987 'Complex permittivity of water between 0 and 30 THz'. Pp. 229–230 in Proceedings of the 12th international conference on infrared and millimeter waves, IEEE, Orlando, Florida

Njoku, E. G. 1995 Surface temperature estimation over land using satellite microwave radiometry. Pp. 509–530 in *Passive microwave remote sensing of land–atmosphere interaction*. Eds. B. J. Choudhury, Y. H. Kerr, E. G. Njoku and P. Pampaloni. Utrecht, The Netherlands

Phalippou, L. 1996 Variational retrieval of humidity profile, wind speed and cloud liquid water path with SSM/I: Potential for numerical weather prediction. *Q. J. R. Meteorol. Soc.*, **122,** 327–355

Prigent, C., Phalippou, L. and English, S. 1997a Variational inversion of SSM/I observations during the ASTEX campaign. *J. Appl. Meteorol.*, **36,** 493–508

Prigent, C., Rossow, W. B. and Matthews, E. 1997b Microwave land surface emissivities estimated from SSM/I observations. *J. Geophys. Res.*, **102,** 21867–21890

1998 Global maps of microwave land surface emissivities: Potential for land surface characterization. *Radio Sci.*, **33,** 745–751

Rodgers, C. D. 1976 Retrieval of atmospheric temperature and composition from remote measurements of thermal radiation. *Rev. Geophys. Space Phys.*, **14,** 609–624

Rosenkranz, P. W. 1992 Absorption of microwaves by atmospheric gases. In *Atmospheric remote sensing by microwave radiometry*. Ed. M. A. Janssen. Wiley-Interscience, New York, USA

Rossow, W. B. and Garder, L. C. 1993a Cloud detection using satellite measurements of infrared and visible radiances for ISCCP. *J. Climate*, **6,** 2341–2369

1993b Validation of ISCCP cloud detections. *J. Climate*, **6,** 2370–2393

Rossow, W. B. and Schiffer, R. A. 1991 ISCCP cloud data products. *Bull. Am. Meteorol. Soc.*, **72,** 2–20

Rossow, W. B., Walker, A. W., Beuschel, D. E. and Roiter, M. D. 1996 'International Satellite Cloud Climatology Project (ISCCP): Document on new cloud datasets'. Available from NASA, Goddard Institute for Space Studies, New York, USA

Sheu, R. S., Curry, J. A. and Liu, G. 1997 Vertical stratification of cloud properties as determined from satellite. *J. Geophys. Res.*, **102,** 4231–4245

Slingo, J. M. 1987 The development and verification of a cloud prediction scheme for the ECMWF model. *Q. J. R. Meteorol. Soc.*, **113,** 899–927

Spencer, R. W., Goodman, H. M. and Hood, R. E. 1989 Precipitation retrieval over land and ocean with the SSM/I: Identification and characteristics of the scattering signal. *J. Atmos. Oceanic Technol.*, **6,** 254–273

Ulaby, F. T., Moore, R. W. and Fung, A. K. 1986 *Microwave remote sensing. Vol. 3: From theory to applications*. Artech House Inc. Dedham, MA, USA

Wang, J. 1996 'Determination of cloud vertical structure from upper air observations and its effects on atmospheric circulation in a GCM'. PhD thesis, School of Arts and Sciences, Columbia University

Wang, J. and Rossow, W. B. 1995 Determination of cloud vertical structure from upper-air observation. *J. Appl. Meteorol.*, **34,** 2243–2258

Wentz, F. J. 1988 'User's manual SSM/I antenna temperature tapes'. RSS Technical Report 032588, Remote Sensing Systems, Santa Rosa, California, USA